ADVANCED OPTICAL MATERIALS
www.advopticalmat.de

Plasmonic Airy Beam Generation by Both Phase and Amplitude Modulation with Metasurfaces

Zhi Li, Hua Cheng, Zhaocheng Liu, Shuqi Chen,* and Jianguo Tian**

The Airy beam represent the only possible nondiffracting wave packets in 1D planar systems with curved trajectory, which has attracted considerable research interest due to its nondiffracting, self-healing properties, and unique self-bending behavior in the absence of any external potential. Because of the complexity of the Airy function and generation structure, an Airy beam with both phase and amplitude modulation is hard to realize. Here, a simplified metasurface composed of orthogonal nanorods is proposed, which can generate plasmonic Airy beams with both phase and amplitude modulation. By changing the configuration of the nanorods, the phase and amplitude can be simultaneously modulated. The bending degree of the generated Airy beam can be easily controlled by changing the number of nanorods. The proposed controllable Airy beam with both phase and amplitude modulation overcomes certain limitations of the customary Airy beam and can aid in the development of more accurate applications of the Airy beam in microfields.

1. Introduction

Bessel beam, as one of the exact solutions of Helmholtz equation, was predicted theoretically and experimentally demonstrated by Durnin et al. in 1987.[1] This discovery inspired the thoughts of exploring more nondiffraction wave profiles conforming to Helmholtz equation. The nondispersion Airy wave packet with curved propagation profile was first predicted by Berry and Balazs within the context of quantum mechanics by demonstrating that the Schrödinger equation could possess an Airy function form solution.[2] Due to the mathematical similarity between the Schrödinger equation and the paraxial Helmholtz equation, the Airy function solution was introduced in the domain of optics by Christodoulides and co-workers in 2007 and has attracted spectacular research interest on account of its peculiar properties and applications.[3,4] Compared with the former nondiffracting beams such as Bessel beam, Airy beam has the remarkable feature of freely accelerating even in the absence of any external potential except for the nondiffracting and self-healing properties. In the past few years, the tremendous application potential of Airy beam has been proposed and demonstrated, such as forming optical bullet,[3] optical micromanipulating,[5] and producing curved plasma channels.[6] However, traditional methods to generate Airy beam usually involve the Fourier transform of lens which needs at least one focus length and thus affects the compactness of optical system.[4,7–9] It is even impossible to implement Airy beam in the integrated optics system with size comparable to wavelength, which limits its application in the field of nanotechnology.

As a new class of metamaterials, metasurfaces which consist of a monolayer of planar structures have shown great promise for producing nearly arbitrary wavefront of electromagnetic waves by engineering structure dependent phase shift with less energy loss.[10,11] Some exotic applications have been demonstrated using metasurfaces, including anomalous refraction,[12–14] ultrathin flat lens,[15,16] perfect absorbance,[17–19] spin-Hall effect of light,[20] and optical polarization conversion of light.[21–23] Based on the idea of metamaterials and metasurfaces, Minovich et al. proposed the phase-modulation method to produce the Airy beam.[24] The small dimension of metamaterials finely solves the difficulty in generating self-accelerated beams in nanoscale. However, due to the complexity of Airy function and nanostructure, it is hardly possible to consider the amplitude modulation at the same time, which damages the profile of Airy beam.[25] Recently, the anomalous refraction and reflection conformed to generalized Snell's Law were achieved by various-shaped nanoantennas.[10,26,27] Generalized optical laws were first demonstrated by using V-shaped optical antennas and later by using reflect-arrays. This provides us with a new tool to simultaneously control amplitude and phase of scattered light by metasurfaces, which can also be utilized to generate nanoscale Airy beam with both phase and amplitude modulation.

Here, we propose a metasurface composed of orthogonal gold nanorods, which can generate Airy beam with both phase and amplitude modulation without inducing too much complexity. By engineering the metasurface-induced phase profile and tuning the length of nanorods at the same time, the phase and amplitude of Airy beam can be readily modulated. We also

Dr. Z. Li, Prof. H. Cheng, Dr. Z. Liu, Prof. S. Chen, Prof. J. Tian
The Key Laboratory of Weak Light Nonlinear Photonics
Ministry of Education
School of Physics and Teda Applied Physics Institute
Nankai University
Tianjin 300071, China
E-mail: hcheng@nankai.edu.cn; schen@nankai.edu.cn; jjtian@nankai.edu.cn
Prof. H. Cheng, Prof. S. Chen, Prof. J. Tian
The 2011 Project Collaborative Innovation Center for Biological Therapy
Nankai University
Tianjin 300071, China

DOI: 10.1002/adom.201600108

present a reasonable way to simplify the amplitude modulation and compare the differences between different amplitude modulations by the nondiffracting, self-bending, and self-healing features of Airy beam. Moreover, the bending degree of the proposed Airy beam can also be easily controlled by changing the number of nanorods.

2. Results and Discussion

To realize the modulation of both phase and amplitude, we introduce the nanorods with different rotation angles ϕ and lengths l as our basic unit to scatter circularly polarized light, as illustrated in **Figure 1**a. The length L and width W of the unit cell are both 500 nm. Figure 1b shows the phase shift of the anomalous light scattered from the gold nanorod as a function of the rotation angle. When a nanorod has a linear rotation along the x-axis from 0° to 180°, the phase shift can cover the entire phase range from 0 to 2π. This phase change is opposite for left-circularly polarized (LCP) and right-circularly polarized (RCP) incident beams.[28–30] Here we just need to specify two rotation angles (0° and 90°) for two specific phase delays (0 and π), as shown in the insets of Figure 1b. The amplitude modulation can be realized by changing the lengths of the nanorod. Figure 1c shows the amplitude transmission of the converted beam for different lengths of the nanorod. It can be fitted by a Gaussian curve (dashed line) $T(x) = A\exp(-(x-B)/C)^2)$, where the coefficients are A = 0.3314, B = 340.4, and C = 103.3, respectively. Figure 1d shows the response frequency and amplitude transmission of anomalous light as a function of the thickness of nanorod. The conversion efficiency can be easily increased by simply increasing the thickness of the nanorod with a simultaneous blue shift in the response wavelength. The maximal conversion efficiency can be reached about 0.25 for the single-layer metasurface. We sacrificed the conversion efficiency to improve the simulated efficiency in the current configuration.

The plasmonic metasurface capable of generating the Airy beam is schematically shown in **Figure 2**a. It consists of arrays of identically shaped gold nanorods along the x-direction, which exhibits a resonance at the wavelength of 2 μm. A period is indicated by a purple rectangle in Figure 2a. The width and thickness of the nanorod are w = 50 nm and t = 10 nm, respectively. The length of nanorod depends on the value of Airy function. The optical constant of gold is $\varepsilon = -158.038 + 21.42i$ at the wavelength of 2 μm.[31] The permittivity of the SiO_2 substrate is taken as 2.25. All numerical simulations were carried out using finite-element method-based commercial software, COMSOL Multiphysics.[32] The RCP plane wave is normally incident onto the metasurface. The incident electric field is set as E_x = 1 V m^{-1} and $Ey = i$ V m^{-1}. The scattering boundary condition is employed on the bottom of the silica substrate. Perfectly matched layers are used at both sides of the x-direction and top of the simulation domain to completely absorb waves, leaving the simulation domain in the direction of propagation. The detected electric field is set as abs($E_x + iE_y$) at the background of the metasurface. Thus, we can only observe the electric field mode of LCP anomalous light and filter out the RCP light. In this way, the generated plasmonic Airy beam can be detected in the x-z plane.

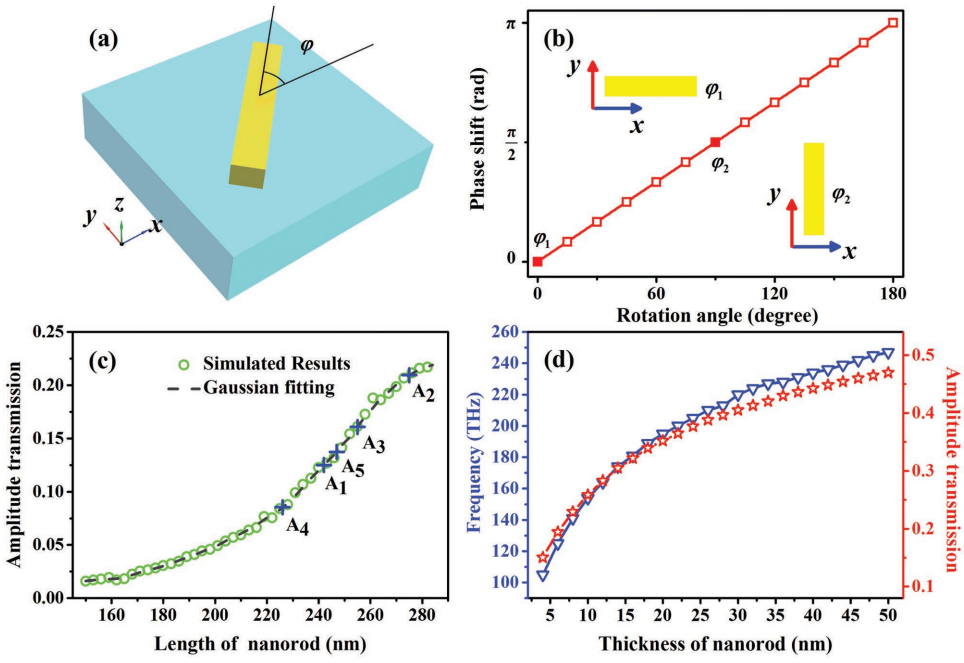

Figure 1. a) A basic unit of gold nanorod. ϕ is the rotation angle of the nanorod relative to the x-axis. b) Phase shift of anomalous light scattered from gold nanorod as a function of rotation angle. Insets: two rotation angles (ϕ_1 = 0° and ϕ_2 = 90°) for two specific phase shifts (0 and π). c) Simulated amplitude transmission (green circles) and fitted Gaussian curve (dashed line) of the anomalous light scattered from gold nanorod for different lengths of the nanorod. Blue markers represent the nanorods with different lengths used in simplified amplitude modulation. d) Response frequency and amplitude transmission of anomalous light as a function of the thickness of nanorod.

Adv. Optical Mater. 2016,
DOI: 10.1002/adom.201600108

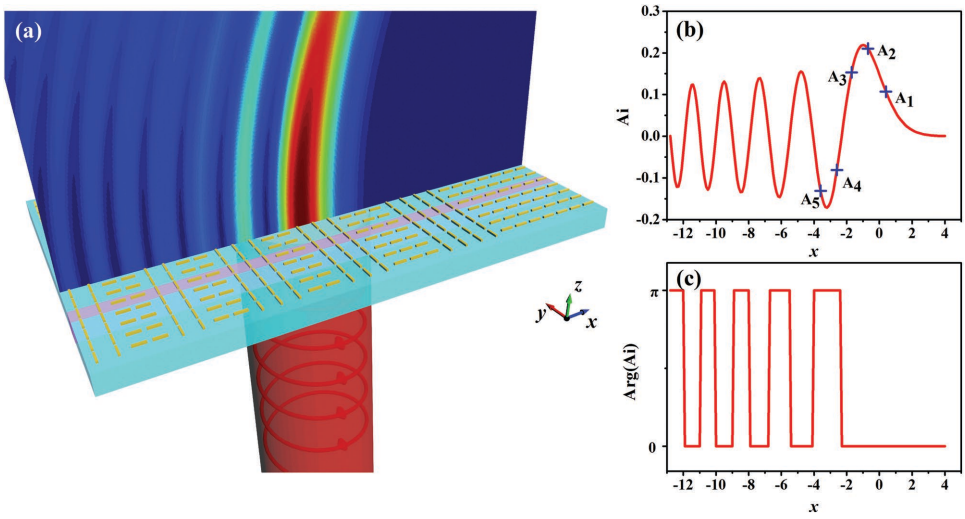

Figure 2. a) Schematic illustration of a representative plasmonic metasurface capable of generating the Airy beam. b) Normalized Airy function. Blue markers represent the amplitude values used in simplified amplitude modulation. c) Phase pattern of the Airy function.

In order to easily determine the geometry parameters of the nanorod, we normalized the Airy function to have the same maximum value as that of the amplitude transmission of the converted beam in Figure 1c. The normalized Airy function is shown in Figure 2b, which clearly exhibits the oscillatory and exponential decaying features. For 1D Airy beam, the phase and displacement are described as follows[33]

$$\phi(x,\theta) = \mathrm{Ai}(bx)\exp(ax + ikbx\sin\theta) \tag{1}$$

where k denotes the wave number, a is a positive value, b is the transverse scale, and θ is the bending direction. The desired phase distribution is introduced: $\varphi = \arg[\phi(x,\theta)] = kbx\sin\theta$ for $\mathrm{Ai}(bx) \geq 0$, and $\varphi = \arg[\phi(x,\theta)] = \pi + kbx\sin\theta$ for $\mathrm{Ai}(bx) < 0$. The bending direction of the generated Airy beam is perpendicular to the metasurfaces when θ is equal to 0. Then, the (0, π) phase profile can be obtained, as shown in Figure 2c. Actually, it is feasible to separately modulate the phase and amplitude by changing the rotation angle and the length of the nanorods. Two types of orthogonal nanorods ($\phi = 0°$ and 90°) can realize the alternative appearing 0 and π phase profile representing $\mathrm{Ai}(x) \geq 0$ and $\mathrm{Ai}(x) < 0$, respectively, which correspond to the oscillatory feature of Airy function. The nanorods with different lengths can describe the exponential decaying feature by averagely dividing the normalized Airy function into 60 segments. Each segment has a transmission amplitude in the normalized Airy function, which corresponds to a specific length for the nanorod in Figure 1c. Thus, the exponential decaying feature can be realized by the nanorods with different lengths.

To compare the influence of the amplitude modulation, we show the electric field distributions of the generated Airy beam for different cases of amplitude modulation in **Figure 3**. The insets of Figure 3 compare the normalized intensities of the generated Airy beams (white lines) with that of the ideal Airy beam (red lines) at 5 μm away from the metasurface. Figure 3a shows the generated Airy beam without amplitude modulation, where only the phase is modulated by two orthogonal nanorods with the same length. Although the self-bending and nondiffracting features seem to be apparent, the spatial spectrum (in the wavenumber space) of the profile in the near field is actually similar to the shape of a rectangular wave.[34] The inset of Figure 3a also shows that the normalized intensity distribution in the near field has a big difference with that of the ideal Airy beam. Its deflection trajectory will deviate the design one due to the excessive approximation. Figure 3b shows the generated Airy beam with full amplitude modulation, where the amplitude is modulated according to the Airy function. The intensity distribution and nondiffracting feature are more reasonable since it does not need to adjust the intensity distribution by the self-healing property. The normalized intensity in the inset of Figure 3b is more consistent with the ideal Airy beam than that in Figure 3a, showing the exponential decaying feature.

It is worth noting that the realization of Airy beam with full amplitude modulation is relatively complicated. We adopt 60 nanorods with different lengths to generate Airy beam, which is not easily achieved from the perspective of nanofabrication. Actually, the exponential decaying feature of the Airy function is also discretized for the Airy beam with full amplitude modulation. We can further reduce the number of the divided segments in the Airy function since the maximal peak values vary a little from the second oscillatory period. The first oscillatory period is divided into five segments (A_1–A_5 as indicated in Figure 2b). We adopt four nanorods with the same length to describe the amplitude for each segment. The other oscillatory periods are described by the nanorods with the same length. Figure 3c shows the generated Airy beam with simplified amplitude modulation, which is identical with the Airy beam with full amplitude modulation (as shown in Figure 3b). The inset of Figure 3c also shows the normalized intensity distribution of the generated Airy beam, which is consistent with the ideal Airy beam and the Airy beam with full amplitude modulation.

In order to further prove the advantages and the validities of the proposed simplified design, we compared three important features for the Airy beam with simplified amplitude

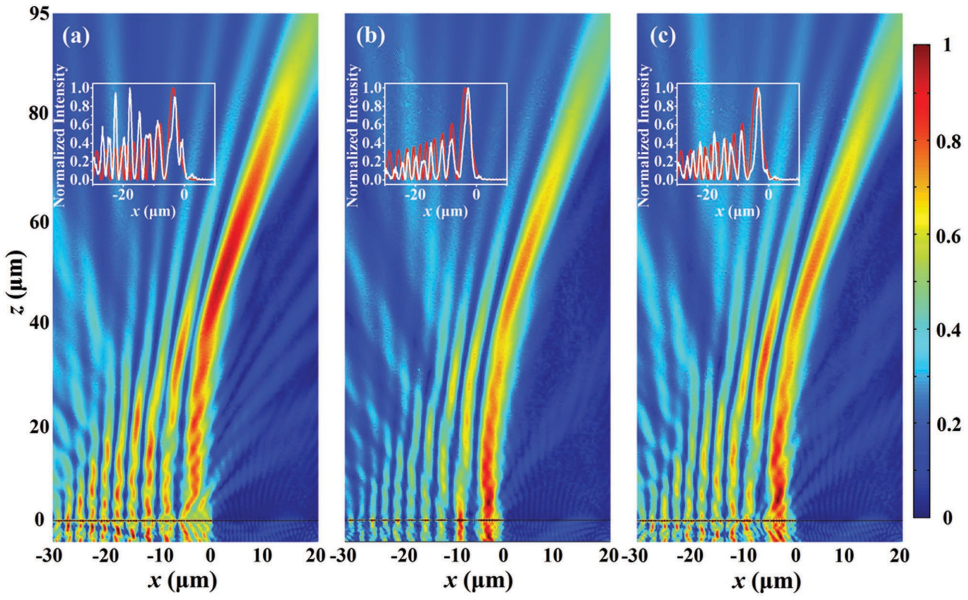

Figure 3. Simulated electric field distributions of the generated Airy beams a) without amplitude modulation, b) with full amplitude modulation, and c) simplified amplitude modulation. Insets: comparison of the normalized intensities between the generated Airy beams (white lines) and the ideal Airy beam (red lines) at 5 μm away from the metasurface.

modulation and without amplitude modulation in the following. The full width at half maximum (FWHM) of the main lobe is a main parameter to evaluate the nondiffracting nature of the Airy beam. **Figure 4**a gives the FWHM for the Airy beams with simplified amplitude modulation and without amplitude modulation. The FWHM for the propagating Airy beam with simplified amplitude modulation remains relatively stable (around 3 μm, between the gray dashed lines) from the beginning to the diffracting zone, which is marked by gray shading (about 56 μm). At the diffracting zone, the FWHM expands quickly and the nondiffracting feature gradually fades out. In the contrast, at the initial stage of propagation (before 5 μm), there are some stronger variations for the Airy beam without amplitude modulation. Moreover, the FWHM has apparent fluctuation throughout the nondiffracting zone. As the transmission amplitudes of the nanorods for the Airy beam without amplitude modulation maintain uniform, the first lobe (each lobe, more generally) can be treated as a diffraction grating. The lobe needs to focus at the initial stage, so the FWHM for the Airy beam without amplitude modulation is much larger

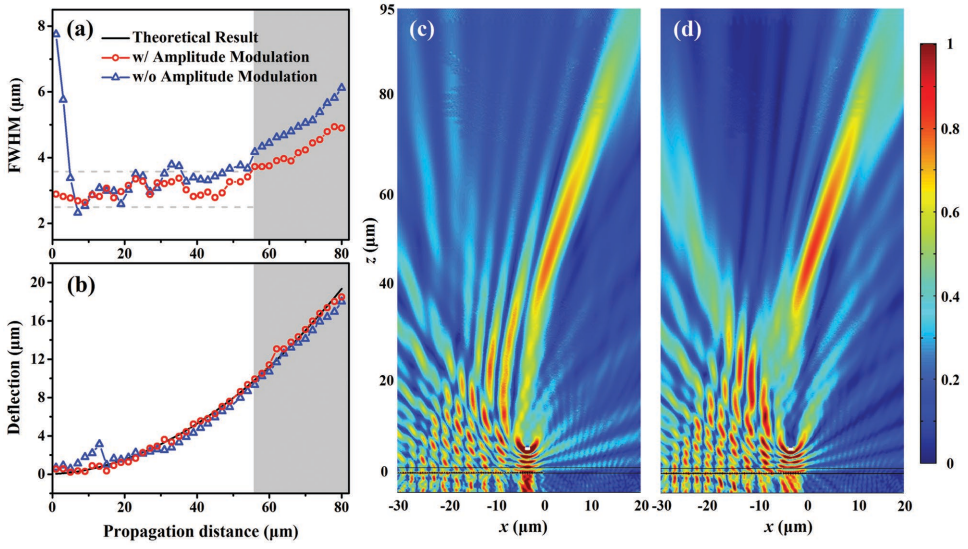

Figure 4. a) FWHM and b) deflection of the main lobe of the Airy beam with simplified amplitude modulation (red line with circles), Airy beam without amplitude modulation (blue line with triangles), and theoretical result (black line) as functions of the propagation distance. Simulated electric field distributions of c) the Airy beam with simplified amplitude modulation and d) Airy beam without amplitude modulation with a rectangular scatterer of the size 1 μm × 0.5 μm centered at $x = -3$ μm and $z = 5$ μm.

Adv. Optical Mater. **2016**,
DOI: 10.1002/adom.201600108

than expected. It is concluded that the Airy beam with simplified amplitude modulation shows better nondiffracting nature and the FWHM is more stable.

The self-bending feature of the Airy beam is also one of the unique inherent attributions. The deflection offset of the main lobe can be well described by the theoretical relation[4]

$$x_d \cong \lambda_0^2 z^2/(16\pi^2 x_0^2) \quad (2)$$

where $x_0 = WN/\alpha$ is an arbitrary transverse scale. W is the unit cell width, N is the number of the nanorods, and $\alpha \approx 14.33$ is the correction factor. This equation can be established when the FWHM of the main lobe remains stable. The deflections of the main lobes for the Airy beams with simplified amplitude modulation and without amplitude modulation together with the theoretical result are shown in Figure 4b. The main lobe of the Airy beam with simplified amplitude modulation follows a smooth trajectory which indicates a good agreement with the theoretical result. While the deflection trajectory of the Airy beam without amplitude modulation has a little deviation from the theoretical result.

To further verify the advantages of the Airy beam with amplitude modulation, we compared the self-healing feature of the Airy beam with simplified amplitude modulation and without amplitude modulation in Figure 4c,d, respectively. A rectangular perfect electric conductor scatterer with the size 1 μm × 0.5 μm centered at $x = -3$ μm and $z = 5$ μm is artificially placed in front of the main lobe. The electric field distributions show that the introduced scatterer only locally disturbs the beams profile, and the beams actually recover after passing scatterer as expected for the nondiffracting beams. Nevertheless, the self-healing feature of the Airy beam with simplified amplitude modulation starts immediately after passing the block while the Airy beam without amplitude modulation is still in chaos, also the side lobes of the Airy beam with simplified amplitude modulation have recovered more integrally. The above differences between two types of generated Airy beams could be explained as follows. The Airy beam without amplitude modulation needs to first correct its field profile along the propagation path, but the scatterer interrupts this process, so it is more interminable; while the Airy beam with simplified amplitude modulation has already adjusted its electric field distribution before encountering the scatterer, so its self-healing feature smoothly occurs after passing the scatterer. The foregoing three featured comparisons further confirmed the validity of the proposed simplified design and proved that the Airy beam with simplified amplitude modulation has greater improvements than the Airy beam without amplitude modulation.

How to control the parabolic trajectory is a wide research topic, since the self-bending feature allows Airy beam itself to be capable of obstacle avoidance. Here we show how to precisely control the propagating trajectory of Airy beam with simplified amplitude modulation. The parabolic trajectory of Airy beam is described by $x_d = az^2$, where the bending parameter a is determined by the ratio of the deflection offset to the propagating distance squared x_d/z^2.[35] Therefore, we can control the deflection offset x_d to affect bending parameter by changing the number of the nanorods. **Figure 5** gives the calculated and simulated bending parameters of the Airy beam

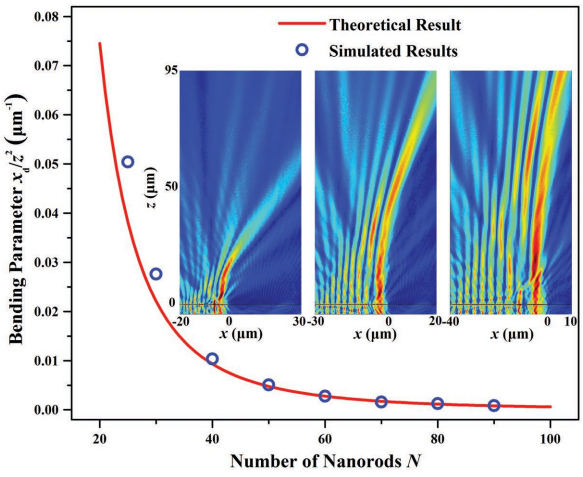

Figure 5. The deflection ratio x_d/z^2 as a function of the number of the nanorods, blue circles refer to the simulated values while the red line represents the theoretical result. Insets: Airy beams for different bending degrees when $N = 40$, 60, and 80.

for different numbers N of the nanorods. With the increasing of the number of the nanorods, the bending parameter is rapidly decreased. When N is less than 30, the simulated bending parameter will gradually deviate the calculated result. Although the large bending parameter can be further obtained by decreasing the number of the nanorods, the oscillatory and exponential decaying features of the Airy function could not be fully described any more. The insets of Figure 5 show the Airy beams for the different bending situations when $N = 40$, 60, and 80, which further confirm that the bending parameter can be controlled by changing the number of the nanorods.

3. Conclusion

The presented metasurfaces finely solve the difficulty in simultaneously controlling amplitude and phase modulation. The simplified approach still remains the features of an Airy beam, which is more valid for nanofabrication. The bending parameter of the Airy beam can be controlled by changing the number of nanorods. However, the metasurfaces need to be designed for each bending parameter. From this perspective, this might be considered as a disadvantage.

In conclusion, we have demonstrated a simplified metasurface which can generate an Airy beam with both phase and amplitude modulation. The advantages of the Airy beam with both phase and amplitude modulation have been discussed in detail. The comparisons of the nondiffracting, self-bending, and self-healing features between the Airy beams with and without amplitude modulation have shown that the Airy beam with amplitude modulation has greater improvements than the Airy beam without amplitude modulation. Moreover, the number of the nanorods can affect the bending parameter of the Airy beam, thus the Airy beam with controllable bending degree can be generated. Our proposed Airy beam with both phase and amplitude modulation may offer a further step forward in more accurate control of the Airy beam to exhibit more applications in microfields.

Acknowledgements

This work was supported by the National Basic Research Program (973 Program) of China (2012CB921900), the Natural Science Foundation of China (11574163, 61378006, and 11304163), the Program for New Century Excellent Talents in University (NCET-13-0294), the International Science and Technology Cooperation Program of China (2013DFA51430), the Natural Science Foundation of Tianjin (13JCQNJC01900), and 111 Project (B07013).

Received: February 22, 2016
Revised: March 17, 2016
Published online:

[1] J. Durnin, J. J. Miceli, J. H. Eberly, *Phys. Rev. Lett.* **1987**, *58*, 1499.
[2] M. V. Berry, N. L. Balazs, *Am. J. Phys.* **1979**, *47*, 264.
[3] G. A. Siviloglou, D. N. Christodoulides, *Opt. Lett.* **2007**, *32*, 979.
[4] G. A. Siviloglou, J. Broky, A. Dogariu, D. N. Christodoulides, *Phys. Rev. Lett.* **2007**, *99*, 213901.
[5] J. Baumgartl, M. Mazilu, K. Dholakia, *Nat. Photonics* **2008**, *2*, 675.
[6] P. Polynkin, M. Kolesik, J. V. Moloney, G. A. Siviloglou, D. N. Christodoulides, *Science* **2009**, *324*, 299.
[7] G. A. Siviloglou, J. Broky, A. Dogariu, D. N. Christodoulides, *Opt. Lett.* **2008**, *33*, 207.
[8] Y. Hu, P. Zhang, C. Lou, S. Huang, J. Xu, Z. Chen, *Opt. Lett.* **2010**, *35*, 2260.
[9] H. T. Dai, X. W. Sun, D. Luo, Y. J. Liu, *Opt. Express* **2009**, *17*, 19365.
[10] N. Yu, P. Genevet, M. A. Kats, F. Aieta, J. P. Tetienne, F. Capasso, Z. Gaburro, *Science* **2011**, *334*, 333.
[11] N. Yu, F. Capasso, *Nat. Mater.* **2014**, *13*, 139.
[12] X. Ni, N. K. Emani, A. V. Kildishev, A. Boltasseva, V. M. Shalaev, *Science* **2012**, *335*, 427.
[13] J. Li, S. Chen, H. Yang, J. Li, P. Yu, H. Cheng, C. Gu, H. Chen, J. Tian, *Adv. Funct. Mater.* **2015**, *25*, 704.
[14] H. Cheng, S. Chen, P. Yu, W. Liu, Z. Li, J. Li, B. Xie, J. Tian, *Adv. Opt. Mater.* **2015**, *3*, 1744.
[15] F. Aieta, P. Genevet, M. A. Kats, N. Yu, R. Blanchard, Z. Gaburro, F. Capasso, *Nano Lett.* **2012**, *12*, 4932.
[16] X. Chen, L. Huang, H. Mühlenbernd, G. Li, B. Bai, Q. Tan, G. Jin, C. W. Qiu, S. Zhang, T. Zentgraf, *Nat. Commun.* **2012**, *3*, 1198.
[17] N. Liu, M. Mesch, T. Weiss, M. Hentschel, H. Giessen, *Nano Lett.* **2010**, *10*, 23428.
[18] N. I. Landy, S. Sajuyigbe, J. J. Mock, D. R. Smith, W. J. Padilla, *Phys. Rev. Lett.* **2008**, *100*, 207402.
[19] S. Chen, H. Cheng, H. Yang, J. Li, X. Duan, C. Gu, J. Tian, *Appl. Phys. Lett.* **2011**, *99*, 253104.
[20] X. Yin, Z. Ye, J. Rho, Y. Wang, X. Zhang, *Science* **2013**, *339*, 14057.
[21] Y. Zhao, M. A. Belkin, A. Alu, *Nat. Commun.* **2012**, *3*, 870.
[22] H. Cheng, S. Chen, P. Yu, J. Li, B. Xie, Z. Li, J. Tian, *Appl. Phys. Lett.* **2013**, *103*, 223012.
[23] H. Cheng, S. Chen, P. Yu, J. Li, L. Deng, J. Tian, *Opt. Lett.* **2013**, *38*, 1567.
[24] A. Minovich, A. E. Klein, N. Janunts, T. Pertsch, D. N. Neshev, Y. S. Kivshar, *Phys. Rev. Lett.* **2011**, *107*, 116802.
[25] Z. Li, K. Yao, F. Xia, S. Shen, J. Tian, Y. Liu, *Sci. Rep.* **2015**, *5*, 12423.
[26] S. Sun, K.-Y. Yang, C.-M. Wang, T.-K. Juan, W. T. Chen, C. Y. Liao, Q. He, S. Xiao, W.-T. Kung, G.-Y. Guo, L. Zhou, D. P. Tsai, *Nano Lett.* **2012**, *12*, 6223.
[27] S. Sun, Q. He, S. Xiao, Q. Xu, X. Li, L. Zhou, *Nat. Mater.* **2012**, *11*, 426.
[28] L. Huang, X. Chen, H. Mühlenbernd, G. Li, B. Bai, Q. Tan, G. Jin, T. Zentgraf, S. Zhang, *Nano Lett.* **2012**, *12*, 5750.
[29] Z. Liu, S. Chen, J. Li, H. Cheng, Z. Li, W. Liu, P. Yu, J. Xia, J. Tian, *Opt. Lett.* **2014**, *39*, 6763.
[30] E. Hasman, Z. Bomzon, A. Niv, G. Biener, V. Kleiner, *Opt. Commun.* **2002**, *209*, 45.
[31] E. D. Palik, *Handbooks of Optical Constants of Solids*, Academic Press, New York **1998**.
[32] *COMSOL Multiphysics User's Guide*, Version number 4.3, Comsol AB, Brulington, MA, USA **2012**.
[33] H. Gao, Z. Gu, B. Liang, X. Zou, J. Yang, J. Yang, J. Cheng, *Appl. Phys. Lett.* **2016**, *108*, 073501.
[34] Z. Lin, X. Guo, J. Tu, Q. Ma, J. Wu, D. Zhang, *J. Appl. Phys.* **2015**, *117*, 104503.
[35] D. M. Cottrell, J. A. Davis, T. M. Hazard, *Opt. Lett.* **2009**, *34*, 2634.